1 *Article*

2 Automated identification of discrepancies between
3 nautical charts and survey soundings

4 **Giuseppe Masetti [1,*], Tyanne Faulkes [2] and Christos Kastrisios [1]**

5   [1]   Center for Coastal and Ocean Mapping/National Oceanic and Atmospheric Administration (NOAA) Joint
6   Hydrographic Center, University of New Hampshire, Durham, NH 03824, USA; gmasetti@ccom.unh.edu,
7   ckastrisios@ccom.unh.edu
8   [2]   National Oceanic and Atmospheric Administration (NOAA) National Ocean Service, Office of Coast
9   Survey, Hydrographic Survey Division, Pacific Hydrographic Branch, Seattle, WA 98115-6349, USA;
10   tyanne.faulkes@noaa.gov
11   *   Correspondence: giuseppe.masetti@unh.edu, Tel.: +1-603-862-3452

13 **Abstract:** Timely and accurate identification of change detection for areas depicted on nautical
14 charts constitutes a key task for marine cartographic agencies in supporting maritime safety. Such
15 a task is usually achieved through manual or semi-automated processes, based on best practices
16 developed over the years requiring a substantial level of human commitment (i.e., to visually
17 compare the chart with the new collected data or to analyze the result of intermediate products).
18 This work describes an algorithm that aims to largely automate the change identification process as
19 well as to reduce its subjective component. Through the selective derivation of a set of depth points
20 from a nautical chart, a triangulated irregular network is created to apply a preliminary tilted-
21 triangle test to all the input survey soundings. Given the complexity of a modern nautical chart, a
22 set of feature-specific, point-in-polygon tests are then performed. As output, the algorithm provides
23 danger-to-navigation candidates, chart discrepancies, and a subset of features that requires human
24 evaluation. The algorithm has been successfully tested with real-world electronic navigational
25 charts and survey datasets. In parallel to the research development, a prototype application
26 implementing the algorithm was created and made publicly available.

27 **Keywords:** nautical cartography; chart adequacy; change detection; triangulated irregular network;
28 safety of navigation; ocean mapping

29

30 1. Introduction

31   The content of a nautical chart is derived from several data sources that can greatly vary in
32 quality and density [1,2]. It is not uncommon to have, in a same nautical chart, parts based on modern
33 high-resolution hydrographic surveys coexist with areas that have not been resurveyed since
34 eighteenth-century lead-line surveys [3]. At the same time, the recent evolution of shipping has both
35 widened and increased the hydrographic needs. New harbors and routes have been established in
36 areas that had never been surveyed [4]. And, on the other side, reasons of economic effectiveness
37 cause merchant vessels to venture into approaches with less under keel clearance than before [3]. In
38 addition, various natural events (e.g., hurricanes, high sedimentation rates) and human activities
39 (e.g., dredging) may modify the condition of the premises and may suddenly make obsolete parts or,
40 in extreme cases, the entirety of a chart [5,6]. Thus, not only the quality of a nautical chart depends
41 on the surveys upon which is derived but surveying for the purpose of keeping nautical charts up to
42 date represents a never-ending task.

43   After a survey, the newly collected datasets are evaluated for evidence of substantial changes
44 against the latest relevant nautical charts. This is an operation that must take into account the
45 numerous transformations that a survey sounding has undergone from the moment that a sonar ping
46 is emitted to its final representation on the chart, in particular when integrated on a statistically-based

bathymetric surface and as the consequence of several possible cartographic adjustments (e.g., rounding and truncation, generalization) [7-10]. In addition, although ontologically distinct, disentangling inaccuracy and uncertainty adds complexity to the already challenging scenario [11]. Concurrently, a general acceleration in the expected rate of change of geospatial information during the past years is contributing to push toward a much shorter updating cycle of nautical charts and, thus, a quick identification of discrepancies for a rapid dissemination of the required nautical information [2,3]. The identification of all the dangers to navigation (DtoNs) and navigationally significant features represents a challenge in complex surveys and significatively contributes to the total processing time of a new dataset [7]. The timely and accurate detection of the above represents a key task for cartographic agencies to fulfill their paramount objective to support the safety of navigation in the relevant waters.

Such a task is complicated by the intrinsic complex nature of a nautical chart that represents the result of a varying combination of human-driven considerations at the compilation time. Those considerations typically change from offshore to inshore, or along an open shoreline toward an intricate estuary [1]. Overall, the main criterion driving the chart compilation is the usefulness to the mariner in relation to the scale of the chart and the surrounding details [1]. Following such a criterion, a less significant feature is generally excluded (or reduced in emphasis) when its insertion may obscure other more important charted features. In areas where detailed depth information is required, a nautical chart provides a careful selection of trend-meaningful charted soundings and depth contours. This selection has the intent to allow the chart user to interpret the morphology of the seabed by interpolating the provided bathymetric information in accordance with the shoal-biased source survey datasets. The nature of the interpolation is delegated to the end user and it can be assumed that this mental process varies from a plain linear interpolation to a heavily biased interpolation toward the conservative side. The degree of bias is a combination of objective and subjective contingent user considerations and, as such, difficult to be estimated. Together with the degree of interpolation bias, the likely existence of a few special cases related to the presence of feature types like marine farms, restricted areas, and other types of obstructions complicates the identification of discrepancies between nautical charts and the survey soundings [12].

The evaluation of current chart adequacy (as well as the rectification of possible deficiencies and shortcomings) represents a world-wide pressing need that poses a challenge to many national hydrographic offices [13,14]. Those offices must balance such a pressing need with the limited available resources and survey priorities that translate to the fact that decades may past until a new hydrographic survey can be conducted in a given area. In such an optic, it is becoming more and more obvious the requirement to evaluate the adequacy of the chart portfolio not only using newly collected bathymetric sonar bathymetry (BSB) but any possible source of geospatial information like automatic-identification system (AIS) data or alternative surveying means like synthetic aperture radar (SAR) shoreline extraction, satellite derived bathymetry (SDB) and airborne-lidar bathymetry (ALB)[6,14-20]. However, given the physically-limited penetration in water of SAR, SDB and ALB or the circular limitation in retrieving information from AIS data (i.e., vessels tend to avoid uncharted areas), BSB surveys – despite their high cost and logistic challenges – not only provide both highly accurate and dense measurements of the seafloor morphology, but also represent the only practical source of hydrographic information for large parts of the ocean [15].

The topic of the identification of nautical chart discrepancies in comparison to newly collected hydrographic survey datasets has received only limited attention in the scientific literature despite its importance to the safety of navigation and relevance in the evaluation of the adequacy of the current charts, as well as for coastal change analysis and coastal zone management [21-24]. In addition, many of the techniques developed for geospatial data analysis on land cannot be straightly applied to the nautical cartography realm mainly because of the peculiar safety of navigation requirement [12,25-28]. Currently, the task to identify chart discrepancies against new BSB data sets is usually performed by the various cartographic agencies through manual or semi-automated processes, based on best practices developed over the years. However, these processes require a

98 substantial level of human commitment that includes the visual comparison of the chart and the new
99 data, and the analysis of the result of intermediate support products.
100 This work describes an algorithm that aims to automate a large extent of the change detection
101 process and to reduce its subjective human component. Through the selective derivation of a set of
102 depth points from a nautical chart, a triangulated irregular network (TIN) is created to apply a
103 preliminary tilted-triangle test to all the input survey soundings. Given the complexity of a modern
104 nautical chart, a set of additional sounding-in-specific-feature tests are then performed. As output,
105 the algorithm provides DtoN candidates, chart discrepancies (the "deep" discrepancies may also be
106 optionally identified), and a subset of features that requires human evaluation (if any). The algorithm
107 has been successfully tested with real-world Electronic Navigational Charts (ENCs) and survey
108 datasets. In parallel to the development of this work, an application implementing the algorithm was
109 created   and   made   publicly   available   in   the   HydrOffice   framework
110 (https://www.hydroffice.org/catools).

2. Materials and Methods

2.1. Electronic Navigational Charts

113 An ENC provides all the information for safe navigation in the form of a database – standardized
114 as to content, structure and format – issued on the authority of government authorized hydrographic
115 offices [29]. As such, it does not only contain information for safe navigation present in the
116 corresponding paper chart but can embed supplementary material present in other kinds of nautical
117 publications (e.g., sailing directions). The ENC content may be directly derived from original survey
118 material, but also from databased information, existing paper charts or a combination of them [30].
119 The International Hydrographic Organization (IHO) has created a standard vector format,
120 named S-57, for official ENCs (that is, produced by a government hydrographic office) that contain a
121 set of data layers for a range of hydrographic applications. However, an IHO S-57 ENC is mainly
122 used, in combination with positional information from navigation sensors and radar data, by an
123 Electronic Chart Display and Information System (ECDIS) to provide a graphical representation of a
124 marine area, including bathymetry and topography, and to assist the mariner in route planning and
125 monitoring by providing natural features, man-made structures, coastlines, and any other
126 information related to marine navigation [6,31]. To meet high standards of reliability and
127 performance, an extensive body of rules defines an ECDIS with the result that, under SOLAS Chapter
128 V regulations, an ECDIS loaded with official ENCs is currently the only alternative for the navigator
129 to the adequate and up-to-date paper charts [32].
130 As defined by the IHO standard, the S-57 data content consists of a set of features that may have
131 a spatial representation in the form of points, lines or polygons. Based on the ENC product
132 specifications, those features must be encoded using the chain-node topology (Figure 1) [31,33]. For
133 a S-57 ENC, the basic unit of geographic coverage is called "cell", normally a spherical rectangle
134 bordered by meridians and latitudes with actual data coverage that can be of any shape [30]. Within
135 the same navigational purpose (e.g., coastal, approach) (Table 1), the cell data may not overlap with
136 those of the adjacent cells. The navigational purpose also drives the compilation scale and, thus, the
137 features contained in a cell.

138
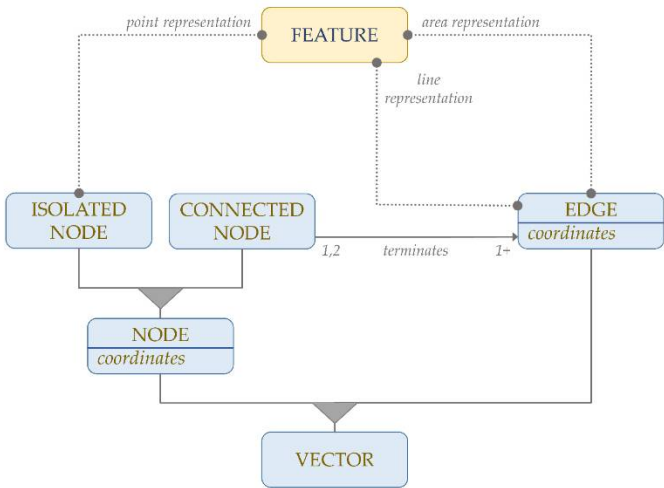
139 Figure 1. Graphical representation of the chain-node topologic model enforced by the S-57 ENC
140 specifications. A geospatial feature may be represented as a point (by an isolated node), a line (using
141 a series of edges and connected nodes), or an area (by a closing loop of edges starting and ending at
142 a common connected node). Vector objects may be shared, but duplication of coincident linear
143 geometry is prohibited [31].

144 Table 1. The ENC navigational purposes with range of compilation scales (and the standard radar
145 scale within each range) suggested by the IHO S-65 publication [30].

ENC Navigation Purpose	Suggested Scale Range	Selectable Radar Range	Rounded Standard Scale
Overview	< 1:1,499,999	200 NM	1:3,000,000
		96 NM	1:1,500,000
General	1:350,000 – 1:1,499,999	48 NM	1:700,000
		24 NM	1:350,000
Coastal	1:90,000 – 1:349,999	12 NM	1:180,000
		6 NM	1:90,000
Approach	1:22,000 – 1:89,999	3 NM	1:45,000
		1.5 NM	1:22,000
Harbour	1:4,000 – 1:21,999	0.75 NM	1:12,000
		0.5 NM	1:8,000
Berthing	> 1:4,000	0.25 NM	1:4,000

146

2.2. Soundings from Bathymetric Sonar Surveys

148 In the hydrographic field, a sounding can be intended as a measured depth of water (i.e., a
149 survey sounding) or as a bathymetric value represented on a nautical chart (i.e., a charted sounding)
150 [29]. The algorithm described in this work digests both kinds of soundings, but with quite distinct
151 uses. In fact, the survey soundings collected using bathymetric sonars – with multibeam sonars
152 (MBES) currently playing a predominant role as acquisition devices – are analyzed as proxies of the
153 bathy-morphology retrieved in a new surveyed area [34], while the charted soundings represent one
154 of the many feature types retrieved from the ENC to reconstruct the bathymetric model that the chart
155 maker wanted to communicate at the time of the ENC compilation (and, when available, after the
156 application of all of the following ENC updates) .
157 The algorithm described in this work was developed to handle as input the following types of
158 survey soundings:

159 • "Pure survey soundings", intended as the point cloud measured by a bathymetric sonar after
160   having been properly integrated with ancillary sensors, cleaned by spurious measurements and
161   reduced to the chart datum.
162 • "Gridded survey soundings", represented by the nodes with valid depth values in a regularly-
163   spaced grid created using the pure survey soundings.
164 • "Selected gridded survey soundings", commonly generated during the cartographic processing
165   using algorithms that select the grid nodes that are more meaningful to depict the trend of the
166   underlining bathymetric model.

167   Assuming the correctness in the generation of the above three types of survey soundings (whose
168 evaluation is outside of the scope of the present work), the algorithm provides similar output results,
169 with the only relevant difference of the number of flagged features. The latter is justified by the
170 different number of survey soundings in input: the gridding and the selection processes commonly
171 reduce the amount of features input of one or more orders of magnitude.

172 *2.3. Bathymetric Model Reconstruction using a Triangulated Irregular Network (TIN)*

173   From a general point of view, a TIN consists of a network of irregular triangles generated by
174 connecting the nodes of a dataset in a way that guarantees the absence of intersecting triangle edges
175 and superposed triangle faces, but also that the union of all the triangles fills up the convex hull of
176 the triangulation (see Figure 2) [35]. For the aims of this work, we generate a TIN from a set of three-
177 dimensional nodes retrieved from the chart and then assume a linear variation of the bathymetric
178 model among those nodes.

179
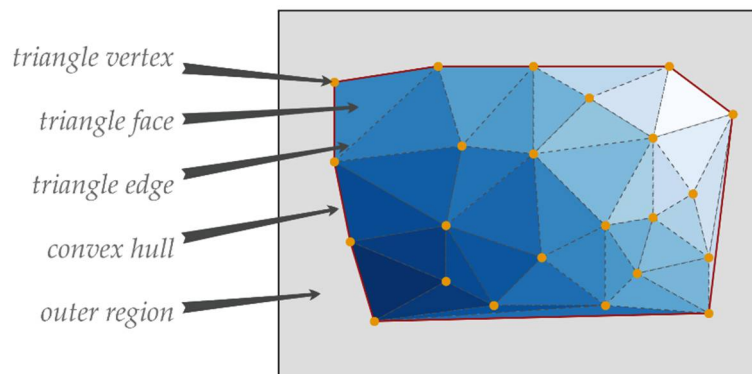
180   Figure 2. Example of a Triangulated Irregular Network (TIN) with the adopted nomenclature for the
181   various components.

182   The generated TIN is based on the Delaunay conforming triangulation [36] selected for the well-
183 known characteristic properties (e.g., being mathematically well defined, providing an unique output
184 for a given dataset independently from the data sequence) [37]. In the literature, several algorithms
185 implementing such a triangulation are available [38,39]. For the present work, we adopted the
186 practical convex hull algorithm that combines the two-dimensional Quickhull algorithm with the
187 general-dimension Beneath-Beyond algorithm, using the implementation provided by the open
188 source QHull code library [40].

189   For the bathymetric model reconstruction, the algorithm retrieves nodes from the following
190 ENC feature types (in parenthesis, the adopted S-57 acronym):
191 • Charted soundings (SOUNDG).
192 • Depth contour lines (DEPCNT) with a valid depth value attribute (VALDCO).
193 • Dredged area polygons (DRGARE) with a valid value for the minimum depth range attribute
194   (DRVAL1).
195 • All the point features with a valid value of sounding attribute (VALSOU).
196 • Natural (COALNE) and artificial (SLCONS) shorelines.
197 • Depth area polygons (DEPARE) for the ENC cell boundaries only.

198   To avoid the creation of triangles crossing feature edges (and, thus, the corresponding
199   misrepresentation in the reconstructed bathymetric model), additional nodes are inserted along the
200   feature edges that are longer than the interpolation length (IL) of one centimeter ($k_{1cm} = 0.01m$) at
201   the ENC compilation scale (CS) (Figure 3):

$$IL = \frac{k_{1cm}}{CS}. \tag{1}$$

202   For example, with a CS value of 1:10,000, the IL obtained by applying (1) is 100 meters.
203   The algorithm retrieves the CS for (1) directly from the ENC, using the value stored in the
204   "Information Scale of Data" (CSCL) subfield in the "Data Set Parameter" (DSPM) field. By definition,
205   such a value represents the compilation scale appropriate to the greater part of the data in the cell
206   [31]. The one-centimeter interpolation value was established as a trade-off value between the
207   requirement of avoiding the triangle-crossing-edge condition and the performance cost paid for a
208   larger point cloud to triangulate. The effectiveness of k_{1cm} has been empirically tested using real-
209   world ENCs, but more conservative values for k – or its derivation from the ENC analysis – may be
210   adopted.

211
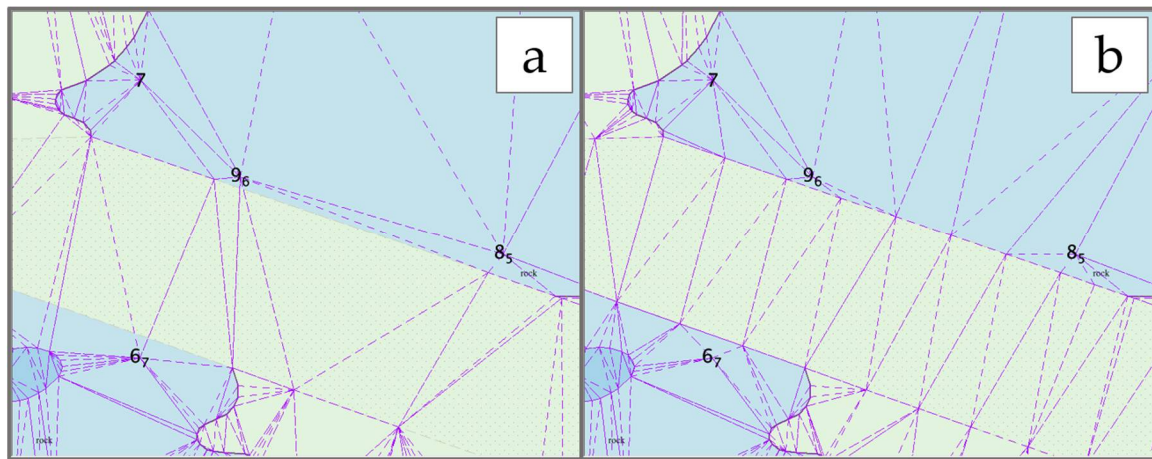
212   Figure 3. Pane (a) shows an example retrieved from an ENC where the long sides of a dredged-area
213   feature (visualized with a dotted pattern) trigger the creation of triangles (dashed magenta lines) that
214   overlap with the same feature edges. After the application of the proposed interpolation criterion, the
215   resulting triangulation shown in pane (b) does not present the overlap issue.

216   In addition to the described point densification, the reconstruction of a bathymetric model from
217   an ENC requires to associate a depth value to the nodes derived from the shoreline features, and that
218   such a value is referenced to the chart vertical datum like all the other depth nodes. Given that chart
219   producers may adopt different methods to identify the shoreline, the algorithm takes the depth value
220   for the shoreline as an input parameter. However, if not provided, the algorithm defaults to use the
221   shallowest depth value among all the valid depth values in the collected nodes.
222   The boundaries of the ENC bathymetry may be defined by the shoreline features and by the cell
223   data limits. In this latter case, based on the enforced chain-node topology, the algorithm retrieves the
224   nodes delimiting the point cloud by intersecting the depth area polygons along the cell boundaries
225   with the depth contour lines. At the resulting nodes is assigned the value of the minimum depth
226   range attribute (S-57 acronym: DRVAL1). In the rare cases where such a value is not populated in the
227   input ENC, the reconstruction of the bathymetric model along those edges cannot be performed and,
228   thus, the evaluation of any survey sounding present in these ambiguous areas is delegated to the
229   analyst.

230   *2.4. Application of the Tilted-Triangle Test*

231   Once the TIN has been generated, the input survey soundings are categorized after the
232   identification of the containing triangle. If a specific survey sounding is outside of all the TIN triangles

233   or is contained within a triangle with all the vertices having the same value (hereinafter referred to
234   as a "flat triangle"), the algorithm temporarily stages it for being re-examined in the step described
235   in the following section.
236   When an input sounding, S, is within a TIN triangle, the algorithm calculates the equation of
237   the tilted plane, $P(x, y, z)$, containing the three triangle vertices, R, S, T:

$$ax + by + cz + d = 0 \qquad (2)$$

238   where:

$$a = \begin{vmatrix} y_S - y_R & z_S - z_R \\ y_T - y_R & z_T - z_R \end{vmatrix},$$

$$b = \begin{vmatrix} z_S - z_R & x_S - x_R \\ z_T - z_R & x_T - x_R \end{vmatrix},$$

$$c = \begin{vmatrix} x_S - x_R & y_S - y_R \\ x_T - x_R & y_T - y_R \end{vmatrix}, \text{ and}$$

$$d = -(ax_R + by_R + cz_R).$$

239   The intersection point, I, between the vertical line, $\boldsymbol{p}$, containing the S point:

$$\boldsymbol{p} = \boldsymbol{t} + \lambda\boldsymbol{v} \qquad (3)$$

240   and the identified P plane is calculated using [41]:

$$\lambda = \frac{-(\boldsymbol{n} \cdot \boldsymbol{t} + d)}{\boldsymbol{n} \cdot \boldsymbol{v}} \qquad (4)$$

241   where $\boldsymbol{n}$ is the normal to the tilted plane:

$$\boldsymbol{n} = a\boldsymbol{i} + b\boldsymbol{j} + c\boldsymbol{k}. \qquad (5)$$

242   The vertical distance, ΔZ_{SI}, is calculated as the difference between the depth dimensions
243   between S and I:

$$\Delta Z_{SI} = z_I - z_S. \qquad (6)$$

244   The algorithm uses the ΔZ_{SI} to evaluate whether flagging the soundings as DtoN candidates
245   (Figure 4) or potential chart discrepancies. The default logic of the applied thresholding (Table 2) is
246   derived from the NOAA Office of Coast Survey (OCS) Hydrographic Surveys Specifications and
247   Deliverables [42]. In deep waters, the DtoN concept does not apply to surface navigation. However,
248   based on the consideration that the presence of a very large discrepancy in comparison to the charted
249   water depth may represent an issue for specific marine operations (e.g., towing a side scan sonar),
250   the algorithm reports – when using default parameters – potential DtoNs for ΔZ_{SI} values larger than
251   the ten percent of the water depth. However, since those values should follow the cartographic
252   organization policy or other types of specific needs, the algorithm is flexible in using customized
253   threshold values.
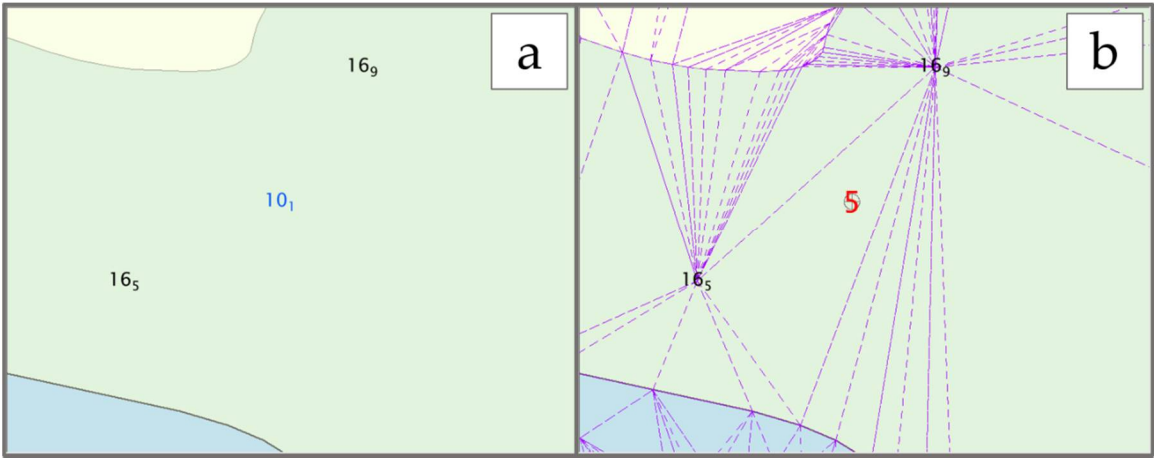
Figure 4. An example of DtoN detection. In the pane (a), a 10.1-meter survey sounding (in blue) is surrounded by two charted soundings (in black) and two depth contours of ten meters and twenty meters. The pane (b) shows the result of the triangulation (dashed lines in magenta) and that the survey sounding was flagged (shown as grey circle) as a DtoN candidate for being about five meters (red value) over the underlying tilted triangle.

Table 2. Default threshold values adopted by the algorithm to identify the DtoN candidates and potential chart discrepancies.

Threshold type	z < 20 meters	z >= 20meters
Danger to Navigation	1.0 meter	10.0 % of water depth
Chart Discrepancy	0.5 meter	5.0 % of water depth

Although large negative ΔZ_{SI} values ("deeps") do not represent a concern from a safety of navigation perspective, their presence provides evidence of chart inconsistencies. As such, the algorithm can be optionally set to identify those deeps, by simply applying a reversed thresholding logic in respect to the "shallow" chart discrepancies.

2.5. Application of the Sounding-in-Specific-Feature Tests

Due to the complexity of a modern nautical chart, the tilted-triangle test alone is not sufficient to properly evaluate all the possible feature configurations that can be depicted on an ENC. As such, the algorithm complements the described in paragraph 2.4 with a set of additional sounding-in-specific-feature tests.

From a geometrical point of view, the first common operation of such tests is to check whether a given sounding point is inside any of the polygons that belong to a specific feature type. Computationally, the detection of the presence of a point inside a polygon is most commonly done using the Ray Casting algorithm [43,44]. Among the several existing implementations available to assess topological relationship between geospatial objects, the algorithm adopted the vectorized binary predicates provided by the Shapely library [45].

A common use case of the point-in-polygon test is provided by the mentioned possible presence of a survey sounding within a flat TIN triangle. A flat triangle can be generated as the result of the triangulation in areas locally characterized by the presence of a linear feature – like a curved depth contour – not closely surrounded by other depth-defined features (Figure 5). In such a case, the algorithm compares the given survey sounding against the validity depth range – when available – of the underlying feature polygon (e.g., a depth area).
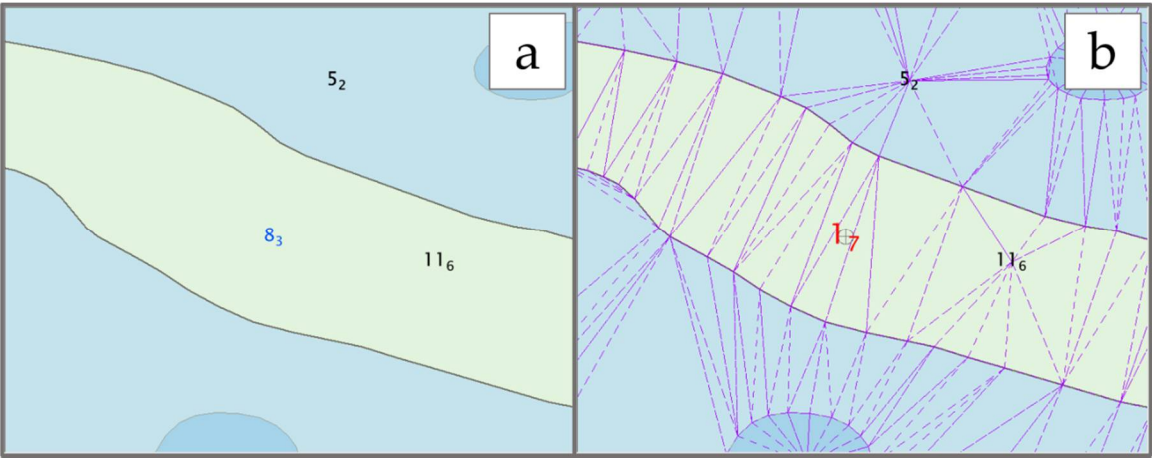
Figure 5. An example of presence of a survey sounding in a flat triangle. In the pane (a), an 8.3-meter survey sounding (in blue) is surrounded by the nodes of a 10-meter depth contour that are closer than the charted soundings (in black). As such, the survey sounding will be contained by a flat triangle (that is, with three vertices having a 10-meter depth) shown in magenta in the pane (b). By adopting the sounding-in-specific-feature test, the algorithm flagged the survey sounding as a potential discrepancy (shown as grey circle with a depth difference of 1.7 meters in red) since it was detected as contained by a depth area with a valid depth range between ten and twenty meters.

The S-57 ENC specifications prescribe that a cell must have the entire area with data covered, without any overlap, by a restricted group of seven area feature types, called the "skin of the earth" (Table 3) [31]. This characteristic of a S-57 ENC contributes to make the sounding-in-specific-feature tests effective to reduce the number of staged untested features. Furthermore, if a survey sounding is not contained in any of the skin of the earth polygons, it is outside of the ENC data coverage and thus does not represent a chart discrepancy.

Table 3. The S-57 ENC area feature types, with the corresponding acronym, belonging to the restricted "skin of the earth" group.

Feature Type	S-57 Acronym
Navigable depth areas	DEPARE
Dredged area	DRGARE
Floating dock	FLODOC
Permanently moored ship	HULKES
Land area	LNDARE
Pontoon	PONTON
Unsurveyed depth area	UNSARE

2.6. Library Implementation, Supporting Visualization, and Output Storage

A software library (current version: 1.0) that implements the algorithm has been developed and tested mostly using the Python language (version 3.6) [46]. For a few selected profiled bottlenecks, a superset of Python, called Cython (version 0.28) [47], was used to reduce the execution time by manually adding a few static type declarations. Using such declarations, Cython was then able to automatically convert Python code into optimized C code.

The library has been coupled with a multi-tab graphical user interface based on a Python port of the Qt framework [48]. The outcomes of the algorithm execution are visualized using the Matplotlib library [49]. ENC-derived depth values are colored by depth, while algorithm-flagged input survey soundings are colored by their discrepancy. If present, the subset of untested input soundings that require human evaluation are displayed with a magenta diamond. The default output is provided in S-57 format using internal code. For easy sorting and identification of discrepancies,

313 the magnitude of the discrepancy against the chart is stored both as cartographic symbol features (S-
314 57 acronym: $CSYMB) and soundings (i.e., storing the discrepancy value as the depth coordinate).
315   Optional output in the popular Shapefile and KML formats are generated using the Geospatial
316 Data Abstraction Library (GDAL) package [50]. In this latter case, the TIN internally used by the
317 algorithm is also generated for debugging aims. An implementation of the algorithm was made
318 publicly available in the HydrOffice framework as a tab widget (Figure 6) freely accessible in the CA
319 Tools application (https://www.hydroffice.org/catools).

320
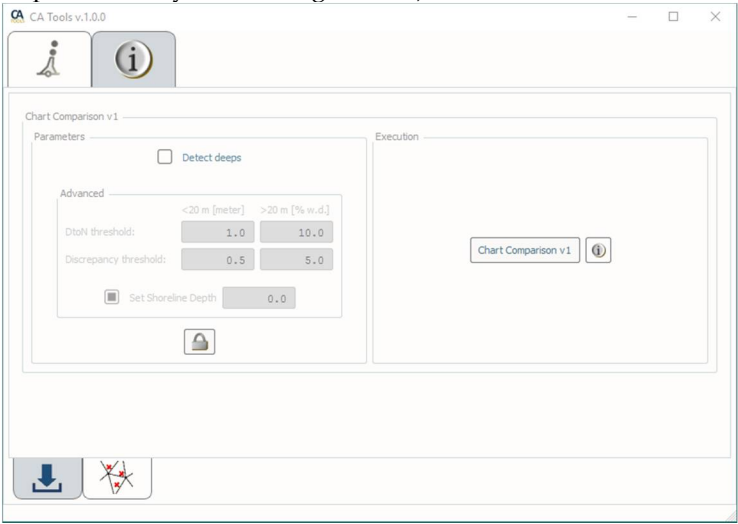
321 Figure 6. Screenshot of the tab widget present in the HydrOffice CA Tools application. The widget
322   exposes, on the left area, the algorithm parameters.

3. Results

324   During the initial development, *ad-hoc* input survey soundings have been generated with two
325 DtoNs and two chart discrepancies to be tested against a valid ENC. Using the described default
326 settings, the algorithm was able to identify both the DtoNs and the chart discrepancies Figure 7.

327
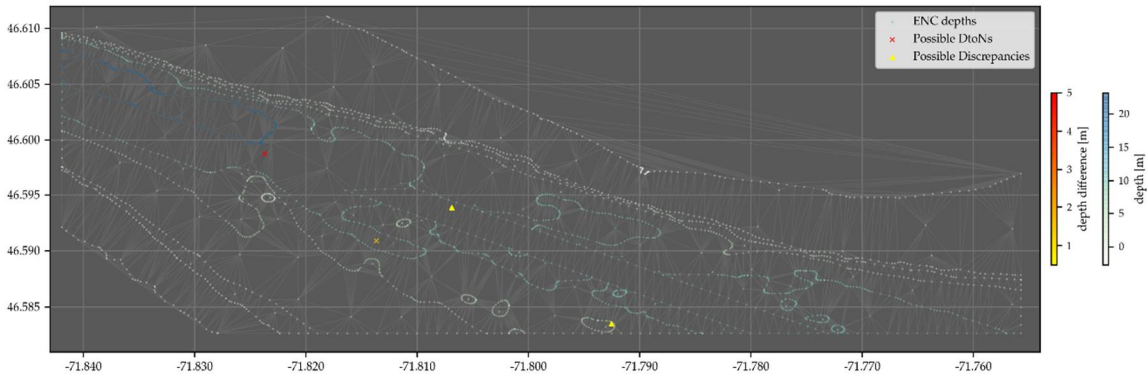
328 Figure 7. Algorithm results when applied to the *ad-hoc* input survey soundings. The possible DtoN
329   are presented using cross markers, while triangular markers are used for the possible discrepancies.
330   The nodes are represented as dots, with the connecting triangle edges in gray. Axes in geographical
331   WGS84 coordinates.

332   The algorithm has then been tested in several real-data scenarios using official ENCs and MBES-
333 based survey datasets. To keep this section concise, only two of those scenarios are here presented.
334 On one side, the analysis of the soundings from NOAA survey H12990 (see Figure 8) shows relatively
335 minor changes to the current ENCs. Conversely, the presence of large active glaciers in the area is
336 highlighted by the analysis of the NOAA H13701 dataset. Further details of the adopted inputs are
337 provided, for the surveys, in Table 4 and, for the ENCs, in Table 5.
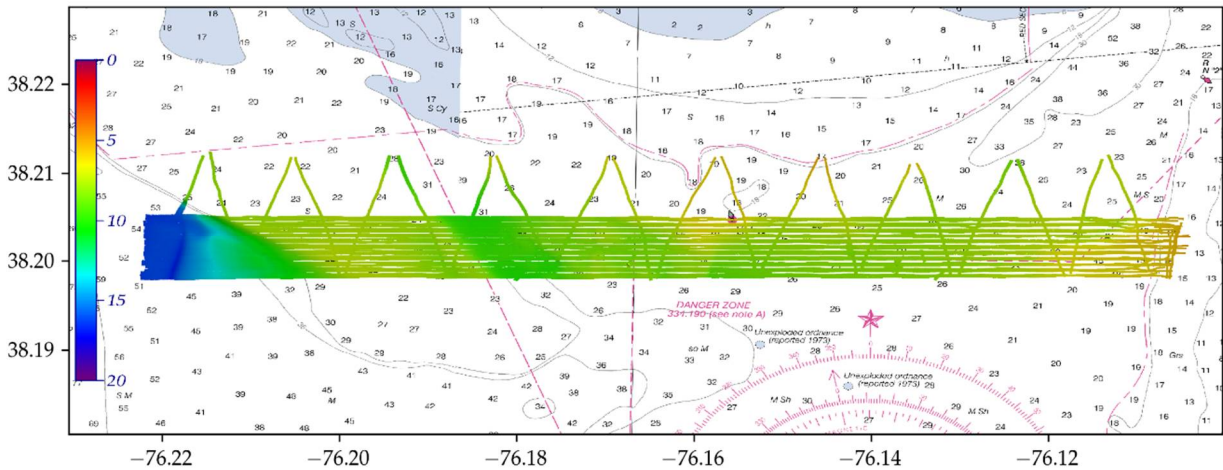
Figure 8. Bathymetric model generated using the data collected by the NOAA H12990 survey. The NOAA raster nautical charts 12331 (Chesapeake Bay Tangier Sound Northern Part) and 12333 (Potomac River Chesapeake Bay to Piney Point) are shown in the background. Bathymetric values in the color bar (in blues) are in meters and referred to the MLLW vertical datum. Axes in geographical WGS84 coordinates.
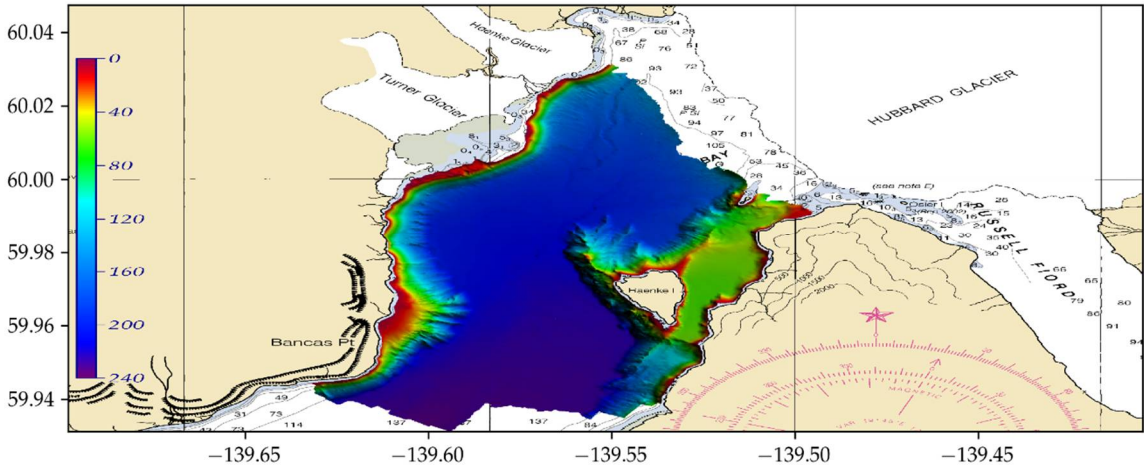
Figure 9. Bathymetric model generated using the data collected by the NOAA H13071 survey. The NOAA raster nautical charts 16761 (Yakutat Bay) is shown in the background. Bathymetric values in the color bar (in blue) are in meters and referred to the MLLW vertical datum. Axes in geographical WGS84 coordinates.

Table 4. Information about the NOAA surveys presented as test datasets.

Survey	Location	Year	Scale	MBES
H12990	Chesapeake Bay (USA)	2017	1:10,000	Kongsberg EM 2040
H13071	Yakutat Bay (USA)	2017	1:40,000	Kongsberg EM 710, Kongsberg EM 2040

Table 5. Information about the NOAA ENCs used to test the algorithm.

Chart	Scale	Edition	Update Number	Issue Date
US5VA21M	1:40,000	21	0	2 May 2018
US5VA22M	1:40,000	28	2	5 June 2018
US4AK3XM	1:80,000	5	0	13 February 2018

352　　　　The results of the analysis for the H12990 survey dataset are shown in Figure 10 and Figure 11.

353
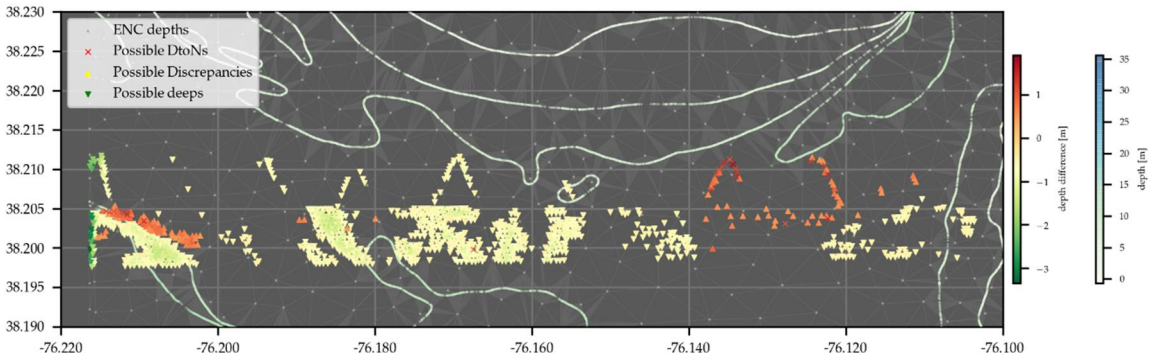
354　　　Figure 10. Algorithm results using the H12990 survey soundings compared to the US5VA21M ENC.
355　　　Axes in geographical WGS84 coordinates.

356
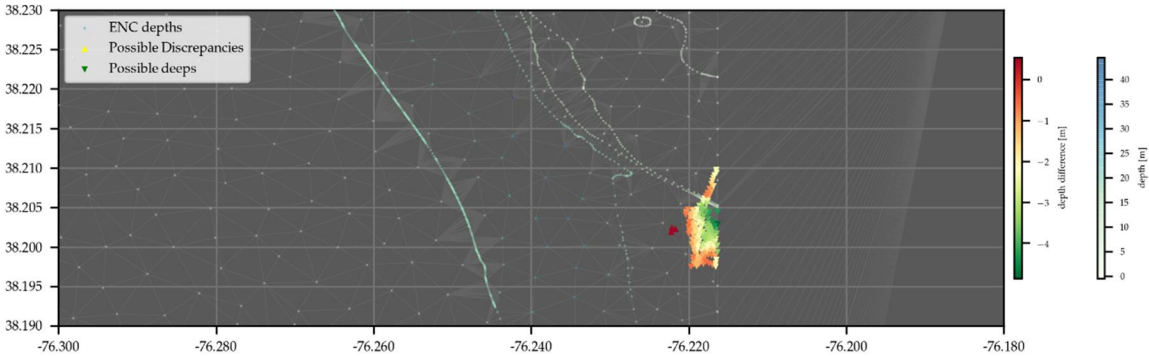
357　　　Figure 11. Algorithm results using the H12990 survey soundings compared to the US5VA22M ENC.
358　　　Axes in geographical WGS84 coordinates.

359　　　　The results of the analysis for the H13701 survey dataset is shown in Figure 12.

360
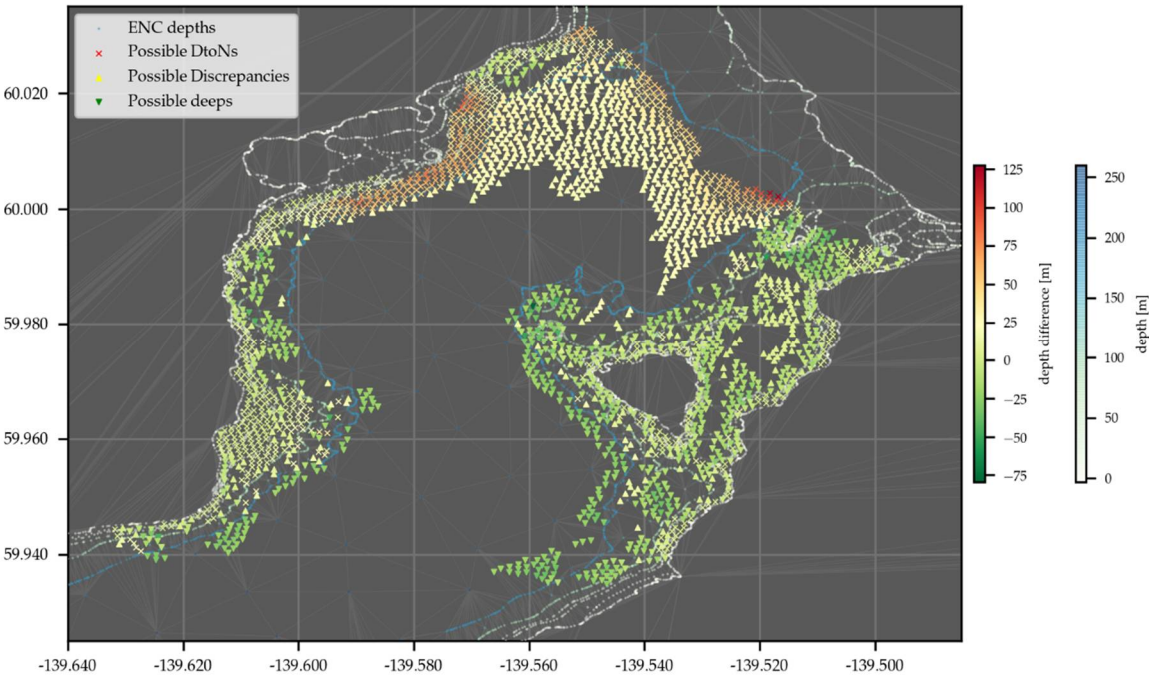
361　　　Figure 12. Algorithm results using the H13701 survey soundings compared to the US5VA22M ENC.
362　　　Axes in geographical WGS84 coordinates.

363 The three applied analyses to the two presented surveys provide results that are consistent with
364 what reported by survey analysts, after a careful but time-consuming evaluation of the same inputs.

4. Discussion

366 Although the algorithm has been successfully tested with several pairs of real-world ENCs and
367 survey datasets, more tests are required to identify possible shortcomings and corner cases absent in
368 the analyzed scenarios. However, the handling of eventual issues will likely happen by extending the
369 described two-step approach and, thus, preserve the general validity of the algorithm proposed in
370 this work.
371 Although popular, the IHO S-57 ENC format is not the only available format to store the
372 geospatial vector information of a nautical chart for use with an ECDIS (e.g., the National Geospatial
373 Agency's Digital Nautical Chart format, the coming IHO S-101 standard) [32,51]. Although this work
374 is based only on ENC data in the IHO S-57 format, the extension to other ENC formats should be
375 straightforward.
376 The survey soundings are ultimately limited by the quality of the original observations used to
377 sample the seafloor [52]. This consideration acquires increasing relevance when the dimensions of
378 the measured chart discrepancies approaches the limits – that should be experimentally evaluated or
379 retrieved by the specifications declared by the manufacturer – of the sonar system used for the survey
380 [53]. The sonar detection uncertainty represents just one potential source of artifacts with a variety of
381 other potential environmental, integration and datum reduction issues that can badly affect the final
382 survey soundings [34,54]. When this happens, bathymetric artifacts generated by the acoustic
383 imaging geometry may be mistaken as chart discrepancies. Among other institutions, the
384 International Hydrographic Organization has developed rules and best practices for the execution of
385 a hydrographic survey that fulfills minimum quality requirements for charting aims [55,56].
386 However, the execution of a hydrographic survey is not always targeted at the production of nautical
387 charts. New hydrographic data are collected for a variety of reasons that spans from scientific
388 research to military applications and marine constructions [57]. Given the high cost of data collection
389 at sea, the national hydrographic offices usually attempt to use those surveys, when made them
390 available, for charting purposes. As such, a buffer representing a lower limit of what is considered a
391 chart discrepancy should also consider an estimation of the soundings quality based on the specific
392 survey being analyzed.
393 A preliminary step in the application of the algorithm consists in the retrieval of the information
394 content present in the input ENC. Ideally, such a content should be used to reconstruct a continuous
395 bathymetric model of the ENC's underwater area that matches – as close as possible – the intent of
396 the chart makers and the expectations of the chart readers. In practice, it is unlikely that, based on
397 different precautionary principles and contingent valuations, two random navigators would draw a
398 perfectly overlapping intermediate contour on a given ENC area. Given the complexity and inherent
399 subjectivity involved in the bathymetric reconstruction, we opted for a simplified, still reasonable
400 solution for the task by generating a TIN from the set of three-dimensional nodes retrieved from the
401 chart and then assuming a linear variation of the model among those nodes.
402 In alternative to the use of the Delaunay conforming triangulation, future works may explore
403 the creation of the TIN based on a constrained Delaunay triangulation [58,59], since this technique
404 makes possible to explicitly define edges ("breaklines") that are not modified by the triangulator
405 (thus removing the currently required addition of interpolated nodes along long edges).
406 The conversion by interpolation of a TIN into a regular grid to perform discrepancy analysis
407 represents a quite popular operation. However, although the several intrinsic advantages related to
408 deal with grid data (e.g., higher processing and development speed) [35], we decided to not take such
409 a direction because of the intrinsic variable-resolution nature of an ENC that makes difficult to
410 identify the best fixed resolution at which to grid the TIN. Regarding the possible creation of a
411 variable-resolution grid, despite the recent development and successful application of this type of
412 gridding algorithms to MBES data [60], a robust estimation of the local resolution based on a ENC-
413 derived data would have been represented a challenge, and it represents an open research question.

414   The described tilted-triangle test represents an evolution of a well-known best practice in
415   nautical cartography for the representation of depth during chart compilation [21]. Such a practice,
416   known as the "triangular method of selection" [61], is commonly used to drive the selection of the
417   charted soundings, and it is based on the following two tests:
418   • Triangle test. Within a triangle of charted soundings, no survey sounding is present which is
419   less than the shallowest depth values defining the corners of the triangle.
420   • Edge test. Between two adjacent charted soundings, no survey sounding exists shallower than
421   the lesser of the two charted soundings.
422   The application of those tests presents some well-known scale- and data density-dependent
423   issues (e.g., which spatial buffer to apply for the edge test? What is the significance of the triangle test
424   with narrow elongated triangles?) that the tilted-triangle test potentially overcomes.

5. Conclusions

426   The present work provides evidence that, with respect to chart adequacy assessment, the
427   adoption of the described two-step algorithm brings several improvements (e.g., less subjectivity and
428   time of execution) in comparison to the current commonly-adopted practices.
429   Future works will focus on exploring techniques to better reconstruct the bathymetric model
430   from ENCs (i.e., attempting to better capture the cartographer and the mariner interpretations of the
431   charted bathymetry) and on evaluating the adoption of the algorithm for chart compilation (as a
432   replacement of the triangle test and the edge test).

434   **Author Contributions:** Methodology and data curation: G.M., T.F. and C.K.; software and visualization: G.M.;
435   formal analysis: G.M. and C.K.; validation, investigation, and resources: T.F.; writing—original draft
436   preparation: G.M.; writing—review and editing: T.F. and C.K.

437   **Funding:** This research was partially funded by the NOAA grant NA15NOS4000200.

438   **Acknowledgments:** Authors would like to thank the NOAA National Ocean Service (NOS) Office of Coast
439   Survey (OCS) and the Canadian Hydrographic Service (CHS) for the datasets, Mathieu Rondeau (CHS
440   Waterways Surveys Unit), Claude Tremblay (CHS Maurice Lamontagne Institute), and Peter Holmberg (NOAA
441   NOS Office of Coast Survey, Pacific Hydrographic Branch) for their support.

442   **Conflicts of Interest:** The authors declare no conflict of interest.

References

444   1.   Russom, D.; Halliwell, H. Some Basic Principles in the Complication of Nautical Charts. *The International*
445   *Hydrographic Review* **1978**, *55*.
446   2.   Mayer, L.; Jakobsson, M.; Allen, G.; Dorschel, B.; Falconer, R.; Ferrini, V.; Lamarche, G.; Snaith, H.;
447   Weatherall, P. The Nippon Foundation—GEBCO Seabed 2030 Project: The Quest to See the World's Oceans
448   Completely Mapped by 2030. *Geosciences* **2018**, *8*, 63, https://doi.org/10.3390/geosciences8020063.
449   3.   Pasquay, J.-N. Safety of modern shipping and requirements in hydrographic surveying and nautical
450   charting. *The International Hydrographic Review* **1986**, *63*.
451   4.   Buixadé Farré, A.; Stephenson, S.R.; Chen, L.; Czub, M.; Dai, Y.; Demchev, D.; Efimov, Y.; Graczyk, P.;
452   Grythe, H.; Keil, K., *et al.* Commercial Arctic shipping through the Northeast Passage: routes, resources,
453   governance, technology, and infrastructure. *Polar Geography* **2014**, *37*, 298-324,
454   https://doi.org/10.1080/1088937X.2014.965769.
455   5.   Masetti, G.; Calder, B. *A Bayesian marine debris detector using existing hydrographic data products*, OCEANS
456   2015 - Genova, 18-21 May 2015, 2015; pp 1-10, https://doi.org/10.1109/OCEANS-Genova.2015.7271584.
457   6.   Roh, J.Y.; Shin, M.S.; Suh, Y.C.; Yang, I.T.; Lee, D.H. Evaluation of Nautical Chart Adequacy in the Coastal
458   Area around Incheon Bay using Satellite Imagery with AIS Data. *Journal of Coastal Research* **2017**, 319-323,
459   https://doi.org/10.2112/SI79-065.1.
460   7.   Moegling, C.; Holmberg, P. *Journey of a Sounding: Application of NOAA Soundings and Features to Navigation*
461   *Products*, U.S. Hydro Conference, New Orleans, LA, USA, 2013; New Orleans, LA, USA, p 17.
462   8.   Calder, B.; Mayer, L. Automatic Processing of High-Rate, High-Density Multibeam Echosounder Data.
463   *Geochemistry Geophysics And Geosystems* **2003**, *4*, https://doi.org/10.1029/2002GC000486.

464   9.   Shea, K.S.; McMaster, R.B. *Cartographic generalization in a digital environment: When and how to generalize,*
465   Proceedings Auto-Carto, 1989; pp 56-67.
466   10.   Gökgöz, T.; Sen, A.; Memduhoglu, A.; Hacar, M. A New Algorithm for Cartographic Simplification of
467   Streams and Lakes Using Deviation Angles and Error Bands. *ISPRS International Journal of Geo-Information*
468   **2015**, *4*, 2185, http://dx.doi.org/10.3390/ijgi4042185.
469   11.   Tucci, M.; Giordano, A. Positional accuracy, positional uncertainty, and feature change detection in
470   historical maps: Results of an experiment. *Computers, Environment and Urban Systems* **2011**, *35*, 452-463,
471   https://doi.org/10.1016/j.compenvurbsys.2011.05.004.
472   12.   James, L.A.; Hodgson, M.E.; Ghoshal, S.; Latiolais, M.M. Geomorphic change detection using historic maps
473   and DEM differencing: The temporal dimension of geospatial analysis. *Geomorphology* **2012**, *137*, 181-198,
474   https://doi.org/10.1016/j.geomorph.2010.10.039.
475   13.   IHO. *C-55: Status of Hydrographic Surveying and Charting Worldwide*; Edition 31 July 2018; International
476   Hydrographic Organization: Monaco, 2018; p 528.
477   14.   Klemm, A.; Pe'eri, S.; Freire, R.; Nyberg, J.; Smith, S.M. *Nautical Chart Adequacy Evaluation Using Publicly-*
478   *Available Data*, U.S. Hydro Conference, National Harbor, MA, USA, 2015; National Harbor, MA, USA, p 6.
479   15.   Chénier, R.; Faucher, M.-A.; Ahola, R. Satellite-Derived Bathymetry for Improving Canadian
480   Hydrographic Service Charts. *ISPRS International Journal of Geo-Information* **2018**, *7*, 306,
481   https://doi.org/10.3390/ijgi7080306.
482   16.   Lyzenga, D.R. Shallow-water bathymetry using combined lidar and passive multispectral scanner data.
483   *International Journal of Remote Sensing* **1985**, *6*, 115-125, https://doi.org/10.1080/01431168508948428.
484   17.   Stumpf, R.P.; Holderied, K.; Sinclair, M. Determination of water depth with high-resolution satellite
485   imagery   over   variable   bottom   types. *Limnology   and   Oceanography* **2003**, *48*, 547-556,
486   https://doi.org/10.4319/lo.2003.48.1_part_2.0547.
487   18.   Su, H.; Liu, H.; Heyman, W.D. Automated Derivation of Bathymetric Information from Multi-Spectral
488   Satellite Imagery Using a Non-Linear Inversion Model. *Marine Geodesy* **2008**, *31*, 281-298,
489   https://doi.org/10.1080/01490410802466652.
490   19.   Pe'eri, S.; Parrish, C.; Azuike, C.; Alexander, L.; Armstrong, A. Satellite Remote Sensing as a
491   Reconnaissance Tool for Assessing Nautical Chart Adequacy and Completeness. *Marine Geodesy* **2014**, *37*,
492   293-314, https://doi.org/10.1080/01490419.2014.902880.
493   20.   Pe'eri, S.; Madore, B.; Nyberg, J.; Snyder, L.; Parrish, C.; Smith, S. Identifying Bathymetric Differences over
494   Alaska's North Slope using a Satellite-derived Bathymetry Multi-temporal Approach. *Journal of Coastal*
495   *Research* **2016**, 56-63, https://doi.org/10.2112/SI76-006.
496   21.   Wilson, M.; Masetti, G.; Calder, B.R. Automated Tools to Improve the Ping-to-Chart Workflow.
497   *International Hydrographic Review* **2017**, *17*, 21-30.
498   22.   Azuike, C.; Pe'eri, S.; Alexander, L.; Parrish, C.; Armstrong, A. *Development of a Geo-spatial Analysis*
499   *Methodology for Assessing the Adequacy of Hydrographic Surveying and Nautical Charts*, Canadian
500   Hydrographic Conference, Niagara Falls, Ontario, Canada, May 15 - May 17, 2012, 2012; Niagara Falls,
501   Ontario, Canada.
502   23.   Moitoret, V.; Johnson, N.E. Automation of Hydrographic Source Data. *The International Hydrographic Review*
503   **1967**, *45*.
504   24.   Furuya, H. Automating the Marine Chart Production Processes. *Cartographica: The International Journal for*
505   *Geographic Information and Geovisualization* **1973**, *10*, 23-36, https://doi.org/10.3138/6716-9222-4534-3440.
506   25.   Qi, H.B.; Li, Z.L.; Chen, J. Automated change detection for updating settlements at smaller-scale maps from
507   updated   larger-scale   maps. *Journal   of   Spatial   Science* **2010**, *55*, 133-146,
508   https://doi.org/10.1080/14498596.2010.487855.
509   26.   Armenakis, C.; Cyr, I.; Papanikolaou, E. Change detection methods for the revision of topographic
510   databases. *Internatioanl Archives of Photogrammetry Remote Sensing and Spatial Information Sciences* **2002**, *34*,
511   792-797.
512   27.   Hussain, M.; Chen, D.; Cheng, A.; Wei, H.; Stanley, D. Change detection from remotely sensed images:
513   From pixel-based to object-based approaches. *ISPRS Journal of Photogrammetry and Remote Sensing* **2013**, *80*,
514   91-106, https://doi.org/10.1016/j.isprsjprs.2013.03.006.
515   28.   Zhang, K.; Whitman, D.; Leatherman, S.; Robertson, W. Quantification of Beach Changes Caused by
516   Hurricane Floyd Along Florida's Atlantic Coast Using Airborne Laser Surveys. *Journal of Coastal Research*
517   **2005**, 123-134, https://doi.org/10.2112/02057.1.
518   29.   IHO. *S-32: Hydrographic Dictionary - English*; International Hydrographic Bureau: Monaco, 1994;
519   http://hd.iho.int/en/index.php/Main_Page.
520   30.   IHO. *S-65: Electronic Navigational Charts (ENCs) "Production, Maintenance and Distribution Guidance"*; Edition
521   2.1.0; International Hydrographic Organization: Monaco, 2017.

31. IHO. *S-57: Transfer standard for digital hydrographic data*; Edition 3.1; International Hydrographic Organization: Monaco, 2000.

32. Alexander, L. Electronic Charts. In *The American Practical Navigator*, National Imaging and Mapping Agency: Bethesda, MD, USA, 2003; pp 199-215.

33. Theobald, D.M. Topology revisited: representing spatial relations. *International Journal of Geographical Information Science* **2001**, *15*, 689-705, https://doi.org/10.1080/13658810110074519.

34. Hughes Clarke, J.E. The Impact of Acoustic Imaging Geometry on the Fidelity of Seabed Bathymetric Models. *Geosciences* **2018**, *8*, 109.

35. De Wulf, A.; Constales, D.; Stal, C.; Nuttens, T. *Accuracy aspects of processing and filtering of multibeam data: grid modeling versus TIN based modeling*, FIG Working week, 2012; pp 6-10.

36. Delone, B. Sur la sphère vide. A la mémoire de Georges Voronoi. *Bull. Acad. Sci. URSS. Cl. Sci. Math.* **1934**, *6*, 793-800, http://mi.mathnet.ru/eng/izv4937.

37. Rebay, S. Efficient Unstructured Mesh Generation by Means of Delaunay Triangulation and Bowyer-Watson Algorithm. *Journal of Computational Physics* **1993**, *106*, 125-138, https://doi.org/10.1006/jcph.1993.1097.

38. Su, P.; Scot Drysdale, R.L. A comparison of sequential Delaunay triangulation algorithms. *Computational Geometry* **1997**, *7*, 361-385, https://doi.org/10.1016/S0925-7721(96)00025-9.

39. Cheng, S.-W.; Dey, T.K.; Shewchuk, J. Algorithms for constructing Delaunay triangulations. In *Delaunay Mesh Generation*, Chapman and Hall/CRC: 2016.

40. Barber, C.B.; Dobkin, D.P.; Huhdanpaa, H. The quickhull algorithm for convex hulls. *ACM Trans. Math. Softw.* **1996**, *22*, 469-483, https://doi.org/10.1145/235815.235821.

41. Vince, J. *Geometry for computer graphics: formulae, examples and proofs*. Springer Science & Business Media: 2006; https://doi.org/10.1007/978-1-84628-997-2.

42. NOAA. *Hydrographic Surveys Specifications and Deliverables*; Edition April 2018; National Oceanic and Atmospheric Administration, National Ocean Service: 2018; p 159.

43. Shimrat, M. Algorithm 112: Position of point relative to polygon. *Commun. ACM* **1962**, *5*, 434, 10.1145/368637.368653.

44. Haines, E. Point in polygon strategies. In *Graphics gems IV*, Paul, S.H., Ed. Academic Press Professional, Inc.: 1994; pp 24-46.

45. Gillies, S.; Bierbaum, A.; Lautaportti, K.; Tonnhofer, O. Shapely: manipulation and analysis of geometric objects. 2007; https://github.com/Toblerity/Shapely.

46. van Rossum, G. *The Python Language Reference: Release 3.6.4*. 12th Media Services: 2018; p 168.

47. Behnel, S.; Bradshaw, R.; Citro, C.; Dalcin, L.; Seljebotn, D.S.; Smith, K. Cython: The Best of Both Worlds. *Computing in Science and Engg.* **2011**, *13*, 31-39, https://doi.org/10.1109/MCSE.2010.118.

48. The Qt Framework. https://www.qt.io/what-is-qt/ (August 2018).

49. Hunter, J.D. Matplotlib: A 2D Graphics Environment. *Computing in Science & Engineering* **2007**, *9*, 90-95, https://doi.org/10.1109/MCSE.2007.55.

50. Warmerdam, F. The Geospatial Data Abstraction Library. In *Open Source Approaches in Spatial Data Handling*, Hall, G.B.; Leahy, M.G., Eds. Springer Berlin Heidelberg: Berlin, Heidelberg, 2008; pp 87-104, https://doi.org/10.1007/978-3-540-74831-1_5.

51. IHO. *S-101 Value Added Roadmatp*; Edition April 2016; International Hydrographic Organization: 2016.

52. Hughes Clarke, J.E. Multibeam Echosounders. In *Submarine Geomorphology*, Micallef, A.; Krastel, S.; Savini, A., Eds. Springer International Publishing: Cham, 2018; pp 25-41, https://doi.org/10.1007/978-3-319-57852-1_3.

53. Lurton, X.; Augustin, J.M. A Measurement Quality Factor for Swath Bathymetry Sounders. *IEEE Journal of Oceanic Engineering* **2010**, *35*, 852-862, https://doi.org/10.1109/JOE.2010.2064391.

54. Masetti, G.; Kelley, J.G.W.; Johnson, P.; Beaudoin, J. A Ray-Tracing Uncertainty Estimation Tool for Ocean Mapping. *IEEE Access* **2018**, *6*, 2136-2144, https://doi.org/10.1109/ACCESS.2017.2781801.

55. IHO. *S-44: Standards for Hydrographic Surveys*; Edition 5; International Hydrographic Organization: Monaco, 2008.

56. IHO. *C-13: Manual Of Hydrography*; Edition 1.04; International Hydrographic Organization: Monaco, 2011.

57. Kastrisios, C.; Pilikou, M. Nautical cartography competences and their effect to the realisation of a worldwide Electronic Navigational Charts database, the performance of ECDIS and the fulfilment of IMO chart carriage requirements. *Marine Policy* **2017**, *75*, 29-37, https://doi.org/10.1016/j.marpol.2016.10.007.

58. Paul Chew, L. Constrained delaunay triangulations. *Algorithmica* **1989**, *4*, 97-108, https://doi.org/10.1007/BF01553881.

59. Hjelle, Ø.; Dæhlen, M. Constrained Delaunay Triangulation. In *Triangulations and Applications*, Springer Berlin Heidelberg: Berlin, Heidelberg, 2006; pp 113-129, https://doi.org/10.1007/3-540-33261-8_6.

580   60.   Calder, B.R.; Rice, G. Computationally efficient variable resolution depth estimation. *Computers &*
581   *Geosciences* **2017**, *106*, 49-59, https://doi.org/10.1016/j.cageo.2017.05.013.
582   61.   IHO. *S-4: Regulations of the IHO for International (INT) Charts and Chart Specifications of the IHO*; Edition 4.6.0;
583   International Hydrographic Organization: Monaco, 2000.
584